

## THERMONUCLEAR REACTION RATES AND PRIMORDIAL NUCLEOSYNTHESIS

CHRISTIAN ILIADIS

*Department of Physics & Astronomy, University of North Carolina at Chapel Hill, NC 27599-3255, USA  
Triangle Universities Nuclear Laboratory (TUNL), Durham, North Carolina 27708, USA*

ALAIN COC

*CNRS/IN2P3, IJCLab, Université Paris-Saclay, Bâtiment, 104, F-91405 Orsay Campus, France*

(Received August 28, 2020)

Submitted to ApJ

### ABSTRACT

Assuming the best numerical value for the cosmic baryonic density and the existence of three neutrino flavors, standard big bang nucleosynthesis is a parameter-free model. It is important to assess if the observed primordial abundances can be reproduced by simulations. Numerous studies have shown that the simulations overpredict the primordial  ${}^7\text{Li}$  abundance by a factor of  $\approx 3$  compared to the observations. The discrepancy may be caused by unknown systematics in  ${}^7\text{Li}$  observations, poorly understood depletion of lithium in stars, errors in thermonuclear rates that take part in the lithium and beryllium synthesis, or physics beyond the standard model. Here, we focus on the likelihood of a nuclear physics solution. The status of the key nuclear reaction rates is summarized. Big bang nucleosynthesis simulations are performed with the most recent reaction rates and the uncertainties of the predicted abundances are established using a Monte Carlo technique. Correlations between abundances and reaction rates are investigated based on the metric of mutual information. The rates of four reactions impact the primordial  ${}^7\text{Li}$  abundance:  ${}^3\text{He}(\alpha, \gamma){}^7\text{Be}$ ,  $d(p, \gamma){}^3\text{He}$ ,  ${}^7\text{Be}(d, p)2\alpha$ , and  ${}^7\text{Be}(n, p){}^7\text{Li}$ . We employ a genetic algorithm to search for simultaneous rate changes in these four reactions that may account for all observed primordial abundances. When the search is performed for reaction rate ranges that are much wider than recently reported uncertainties, no acceptable solutions are found. Based on the currently available evidence, we conclude that it is highly unlikely for the cosmological lithium problem to have a nuclear physics solution.

*Keywords:* methods: numerical — nuclear reactions, nucleosynthesis, abundances — primordial nucleosynthesis

arXiv:2008.12200v1 [astro-ph.CO] 27 Aug 2020

## 1. INTRODUCTION

The standard model of the big bang rests on the three observational pillars of big bang nucleosynthesis (Gamow 1948; Cyburt et al. 2016; Mathews et al. 2017), cosmic expansion (Riess et al. 1998; Peebles & Ratra 2003), and cosmic microwave background radiation (Spergel et al. 2007; Planck Collaboration et al. 2016). Primordial nucleosynthesis took place during the first 20 minutes after the big bang and probes the cosmological model at early time. Nucleosynthesis in the early universe proceeded at temperatures and densities below 1 GK and  $10^{-5}$  g/cm<sup>3</sup>, respectively. It produced the nuclides <sup>1</sup>H (or H), <sup>2</sup>H (or D), <sup>3</sup>He, <sup>4</sup>He, and <sup>7</sup>Li, which represent the building blocks for the subsequent evolution of matter in the universe.

Primordial abundances have been measured in the proper astrophysical site with high precision in recent years. The cosmological deuterium abundance is determined by observing damped Ly- $\alpha$  systems at high redshift, resulting in a primordial number abundance ratio relative to hydrogen of  $(\text{D}/\text{H})_p^{\text{obs}} = (2.527 \pm 0.030) \times 10^{-5}$  (Cooke et al. 2018). The nuclide <sup>3</sup>He has not been observed outside of the Galaxy since its abundance is very small. Also, the galactic chemical evolution of <sup>3</sup>He is uncertain because it is both produced and destroyed inside stars. Therefore, only an upper limit has been established from observations,  $(^3\text{He}/\text{H})_p^{\text{obs}} \leq (1.1 \pm 0.2) \times 10^{-5}$  (Banja et al. 2002). The primordial <sup>4</sup>He abundance is deduced from measurements of metal-poor extragalactic H II regions, resulting in a nucleon fraction of  $Y_p^{\text{obs}} = 0.2449 \pm 0.0040$  (Aver et al. 2015). The cosmological <sup>7</sup>Li abundance is estimated from observations of low-metallicity stars in the halo of the Galaxy, where the lithium abundance is nearly independent of metallicity. The result is  $(^7\text{Li}/\text{H})_p^{\text{obs}} = (1.58 \pm 0.31) \times 10^{-10}$  (Sbordone et al. 2010). The uncertainties for the measured primordial <sup>2</sup>H, <sup>4</sup>He, and <sup>7</sup>Li abundances correspond to values of 1.2%, 1.6%, and 19.6%, respectively. These values are uncorrelated since each of these nuclides is observed in different astronomical objects by independent measurement techniques. The observations will be most useful for constraining cosmology if predicted primordial abundance uncertainties can be reduced to a level similar to that of the experimental ones.

The precision in the cosmological parameters entering the model of big bang nucleosynthesis has also been improved significantly in recent years. In particular, the measurement of anisotropies in the cosmic microwave background radiation has determined the cosmic baryonic density,  $\Omega_b \cdot h^2 = 0.02233 \pm 0.00015$  (Aghanim et al. 2018), with a precision of less than 1%. If we assume, in addition,  $N_\nu = 3$  for the number of neutrino fla-

vors, the standard model of big bang nucleosynthesis becomes a parameter-free theory. These results establish the expansion rate of the early universe and the prevailing thermodynamic conditions (i.e., temperature and density). All that is required to simulate the primordial abundances is to numerically solve the network of coupled differential equations describing the abundance evolution of the light nuclides. The numerical results depend sensitively on the magnitudes and associated uncertainties of the thermonuclear reaction and weak interaction rates (see, e.g., Serpico et al. (2004)).

Many studies (Schramm & Turner 1998; Steigman 2007; Olive 2010; Tanabashi et al. 2018) have found that the predicted primordial abundances, with one exception, conform broadly with the experimental values. This result is significant because the abundances span nine orders of magnitude. Consequently, big bang nucleosynthesis is a sensitive tool for probing the physics of the early universe as well as for constraining physics beyond the standard model (Iocco et al. 2009). The exception is the primordial <sup>7</sup>Li abundance for which the simulated value exceeds the observational result by a factor of about three. This is the *cosmological lithium problem* and it has not found a satisfactory solution yet. The discrepancy may be caused by unknown systematics in the <sup>7</sup>Li observations, poorly understood depletion of lithium in stars, errors in thermonuclear rates of reactions that take part in the lithium and beryllium synthesis, or physics beyond the standard model. Solutions involving exotic physics almost always lead to an overproduction of deuterium incompatible with observations (Olive et al. 2012; Kusakabe et al. 2014; Coc et al. 2015). Solutions involving stellar physics require a uniform *in situ* lithium depletion (Michaud et al. 1984; Korn et al. 2006) over wide metallicity and effective surface temperature ranges (Aguado et al. 2019; Spite et al. 2015). See Fields (2011); Cyburt et al. (2016); Fields et al. (2020); Davids (2020) for reviews.

The goal of this work is to investigate the nuclear physics aspects of this persistent problem. In Section 2, we summarize the most recent information regarding the thermonuclear rates of key reactions. Our reaction network, thermodynamic conditions, and initial abundances are discussed in Section 3. Results from a network Monte Carlo procedure are presented in Section 4. In Section 5, we study correlations between reaction rates and simulated abundances. A genetic algorithm is employed in Section 6 to investigate whether simultaneous rate changes of key nuclear reactions can account for the observed primordial abundances. A concluding summary is given in Section 7. In the Appendix, we

provide information on the rates of selected nuclear reactions.

## 2. NUCLEAR PROCESSES: BAYESIAN REACTION RATES

The twelve most relevant nuclear processes taking part in primordial nucleosynthesis are listed in column 1 of Table 1, together with their rate uncertainty at 1 GK (column 2), the reference for the rates adopted here (column 3), and comments on the data treatment (column 4).

The rates of the weak interactions that convert neutrons to protons, and vice versa,  $n \leftrightarrow p$ , have recently been discussed and computed by Pitrou et al. (2018), who took into account the effects of radiative corrections (including the effects of finite nucleon mass, finite temperature, weak magnetism, quantum electrodynamics, and incomplete neutrino decoupling). The weak rates scale inversely with the free-neutron lifetime<sup>1</sup>, for which we adopt a value of  $\tau = 879.7 \pm 0.8$  s, and, thus, have an uncertainty of  $\leq 0.1\%$ .

The  $p(n,\gamma)d$  reaction rate has been calculated precisely using effective field theory (Ando et al. 2006). The model parameters were constrained, using a Markov chain Monte Carlo procedure, by cross section data for neutron capture, deuteron photodissociation, and photon analyzing powers. The reported rate uncertainty is 0.4%.

Ten reactions listed in Table 1 have been measured directly in the laboratory at the energies of astrophysical interest. The rates for the  ${}^3\text{He}(n,p)t$ ,  $t(\alpha,\gamma){}^7\text{Li}$ , and  ${}^7\text{Li}(p,\alpha)\alpha$  reactions are adopted from Descouvemont et al. (2004). These were obtained using frequentist statistics and  $\chi^2$  optimization, with the implicit assumption of normal likelihoods and approximate treatments of systematic uncertainties. The reported rate uncertainties for these three reactions amount to 1.6%, 4.3%, and 2.5%, respectively. These are small enough that they do not impact big bang nucleosynthesis predictions.

The cross section data for the remaining seven reactions have been analyzed recently using Bayesian hierarchical models. For  $d(p,\gamma){}^3\text{He}$ ,  $d(d,n){}^3\text{He}$ ,  $d(d,p)t$ , and  ${}^3\text{He}(\alpha,\gamma){}^7\text{Be}$ , microscopic theories of nuclear reactions provided the cross section energy dependence, while the absolute cross section normalization was found from fitting the data within the Bayesian framework (Iliadis

et al. 2016; Gómez Iñesta et al. 2017). For  ${}^3\text{He}(d,p)\alpha$ ,  $t(d,n)\alpha$ , and  ${}^7\text{Be}(n,p){}^7\text{Li}$ , R-matrix theory was implemented into the Bayesian model to fit the data (de Souza et al. 2019b,a, 2020). The Bayesian method provides statistically rigorous rate probability densities that can be used in Monte Carlo reaction network studies to derive meaningful simulated primordial abundance uncertainties.

Fields et al. (2020) prefer to “use smooth polynomial fits to the data...by construction this ensures that the fits match the data as well as possible given the uncertainties.” In the present work, we instead prefer to use for our adopted rates (Table 1) well-established nuclear theory (microscopic models or R-matrix theory) as a foundation for the data analysis. We are not implying that one method is superior to the other, only that there is a range of reasonable options. We also prefer to adopt rates obtained using Bayesian techniques because they allow for a rigorous inclusion of statistical and systematic sources of uncertainties in the data analysis. For a recent example of such a study, see the analysis of  ${}^7\text{Be}(n,p){}^7\text{Li}$  data by de Souza et al. (2020).

A few other reaction rates that impact primordial nucleosynthesis, e.g., for  $d(n,\gamma)t$ ,  ${}^3\text{He}(t,d)\alpha$ , and  ${}^7\text{Be}(d,p)2\alpha$ , have been adopted from the literature. They are listed in Table 1 and will be discussed in the text below and in the Appendix. The rates of all other reactions in our network (see Section 3) have been adopted from statistical nuclear model calculations. See Sallaska et al. (2013) for details. We assigned a factor of 10 uncertainty to the latter rates.

## 3. REACTION NETWORK, THERMODYNAMIC CONDITIONS, AND INITIAL ABUNDANCES

We compute primordial nucleosynthesis using a reaction network consisting of 50 nuclides, ranging from  $p$ ,  $n$ ,  ${}^4\text{He}$ , to  ${}^{22}\text{F}$ . These are linked by 466 nuclear processes, such as particle captures, weak interactions, light-particle reactions, etc. Thermonuclear reaction rates are adopted from STARLIB v6.8 (04/2020).<sup>2</sup> The library is in tabular format and lists reaction rates and rate factor uncertainties on a grid of temperatures between 1 MK and 10 GK (Sallaska et al. 2013). Except for a few recently updated reaction rates (see text), the network is similar to the one used by Pitrou et al. (2018).

Assuming that the baryonic density is known (Section 1), the thermodynamic conditions (temperature and density) in the early universe are determined by the expansion rate. The evolutions of temperature and den-

<sup>1</sup> This value is based on the results of seven experiments compiled by the Particle Data Group (Tanabashi et al. 2018) and three more recent measurements (Serebrov et al. 2018; Pattie et al. 2018; Ezhov et al. 2018). A slightly different value of  $\tau = 879.5 \pm 0.8$  s was used in Pitrou et al. (2018).

<sup>2</sup> The STARLIB site has moved to <https://starlib.github.io/Rate-Library/>.

**Table 1.** Main nuclear processes in primordial nucleosynthesis.<sup>a</sup>

Process	Uncertainty (%) <sup>b</sup>	Most recent reference	Comments
$n \leftrightarrow p$	0.09	Pitrou et al. (2018)	theory and neutron lifetime
$p(n,\gamma)d$	0.4	Ando et al. (2006)	MCMC analysis of data
$d(p,\gamma)^3\text{He}$	3.7	Iliadis et al. (2016)	Bayesian data analysis
$d(d,p)t$	1.1	Gómez Iñesta et al. (2017)	Bayesian data analysis
$d(d,n)^3\text{He}$	1.1	Gómez Iñesta et al. (2017)	Bayesian data analysis
$^3\text{He}(n,p)t$	1.6	Descouvemont et al. (2004)	$\chi^2$ data fitting
$^3\text{He}(d,p)\alpha$	1.2	de Souza et al. (2019b)	Bayesian data analysis
$t(d,n)\alpha$	0.3	de Souza et al. (2019a)	Bayesian data analysis
$^3\text{He}(\alpha,\gamma)^7\text{Be}^c$	2.4	Iliadis et al. (2016)	Bayesian data analysis
$t(\alpha,\gamma)^7\text{Li}$	4.3	Descouvemont et al. (2004)	$\chi^2$ data fitting
$^7\text{Be}(n,p)^7\text{Li}$	2.1	de Souza et al. (2020)	Bayesian data analysis
$^7\text{Li}(p,\alpha)\alpha$	2.5	Descouvemont et al. (2004)	$\chi^2$ data fitting

<sup>a</sup>The symbols p, d, t, and  $\alpha$  denote the nuclides  $^1\text{H}$ ,  $^2\text{H}$ ,  $^3\text{H}$ , and  $^4\text{He}$ , respectively.

<sup>b</sup>Rate uncertainty at 1 GK.

<sup>c</sup>See Section A.3.

**Table 2.** Other nuclear reactions in primordial nucleosynthesis considered in the present work.<sup>a</sup>

Process	Uncertainty <sup>b</sup>		Most recent reference
	Reported <sup>c</sup>	Adopted <sup>d</sup>	
$d(n,\gamma)t^e$	8.0%	factor 2	Nagai et al. (2006)
$^3\text{He}(t,d)\alpha^f$	30%	factor 10	Caughlan & Fowler (1988)
$^7\text{Be}(d,p)2\alpha^g$	factor 3	factor 3	Rijal et al. (2019a)

<sup>a</sup>The symbols p, d, t, and  $\alpha$  denote the nuclides  $^1\text{H}$ ,  $^2\text{H}$ ,  $^3\text{H}$ , and  $^4\text{He}$ , respectively.

<sup>b</sup>Rate uncertainty at 1 GK.

<sup>c</sup>Reported in original work.

<sup>d</sup>Adopted here.

<sup>e</sup>See Section A.1.

<sup>f</sup>See Section A.2.

<sup>g</sup>See Section A.4.

sity, adopted from Pitrou et al. (2018), are presented in Figure 1. We start the network calculations at a time of 1.0 s after the big bang, indicated by the vertical dashed lines in both panels. At that time, the temperature and density amount to  $T = 9.93$  GK and  $\rho = 0.0537$  g/cm<sup>3</sup>,

respectively. We end each calculation at a time of  $10^5$  s after the big bang.

The last ingredients needed for setting up the reaction network are the neutron and proton nucleon fractions at the beginning of the calculation. For times  $t \leq 0.1$  s, with temperatures of  $T \geq 30$  GK, all particles (photons, electrons, positrons, protons, neutrons, neutrinos, and antineutrinos) are in thermal equilibrium and the neutron-to-proton number abundance ratio is given by the Boltzmann distribution,  $N_n/N_p = \exp(-Q/kT)$ , where  $Q = 1.29333205(48)$  MeV is the energy equivalent of the neutron-proton mass difference (Mohr et al. 2016) and  $k$  is the Boltzmann constant. As the universe expands and cools, neutrons and protons fall out of equilibrium because the weak rates ( $n + \nu \leftrightarrow p + e^-$ ,  $n \leftrightarrow p + e^- + \bar{\nu}$ ,  $n + e^+ \leftrightarrow p + \bar{\nu}$ ) become comparable to, and then slower than, the expansion rate. Consequently, the neutron and proton abundances freeze out and their ratio continues to change as a result of free neutron decay. Figure 2 displays the nucleon fractions of protons and neutrons as solid and long-dashed lines, respectively. The vertical dashed line indicates the time at which we start the network calculations, when the neutron and proton nucleon fractions are  $X_n = 0.23948$  and  $X_p = 0.76052$ , respectively.

Primordial nucleosynthesis starts about 100 s after the big bang, when the temperature has declined to about

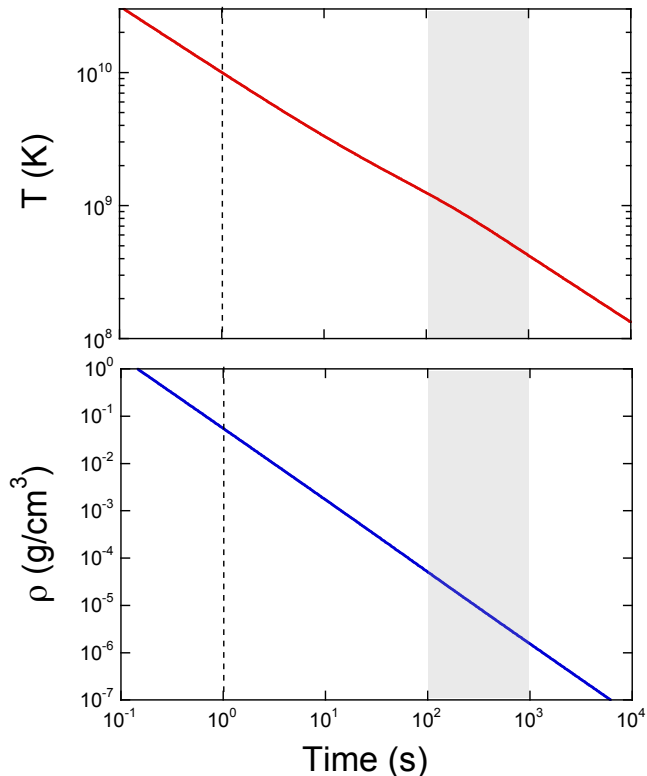


**Figure 1.** Temperature (top) and density (bottom) evolution of the early universe. We start each reaction network calculation at time  $t = 1$  s after the big bang (vertical dashed lines). The most significant primordial nucleosynthesis occurs between 100 s and 1000 s (shaded regions). Results are adopted from [Pitrou et al. \(2018\)](#).

1 GK. This temperature is sufficiently low for the first nuclear reaction,  $p(n,\gamma)d$ , to become faster than its reverse photodisintegration, which until this point prevented the production of heavier nuclei. The nuclear transformations result mainly in the synthesis of  ${}^4\text{He}$ , because it has the highest binding energy among all hydrogen and helium nuclides. It becomes the most abundant species (after  ${}^1\text{H}$ ), while all other nuclides are produced with much smaller abundances. The nucleosynthesis continues until about 1000 s after the big bang (shaded regions in Figure 1). For later times, the temperature and density in the early universe were too small for thermonuclear reactions to change primordial abundances.

#### 4. SIMULATED ABUNDANCES: MONTE CARLO STUDIES

We will next investigate the answer to the following question: *Given a set of recommended reaction rates and their uncertainties, and assuming that these were obtained by taking into account all known statistical and systematic effects in the measured data, what are the best*

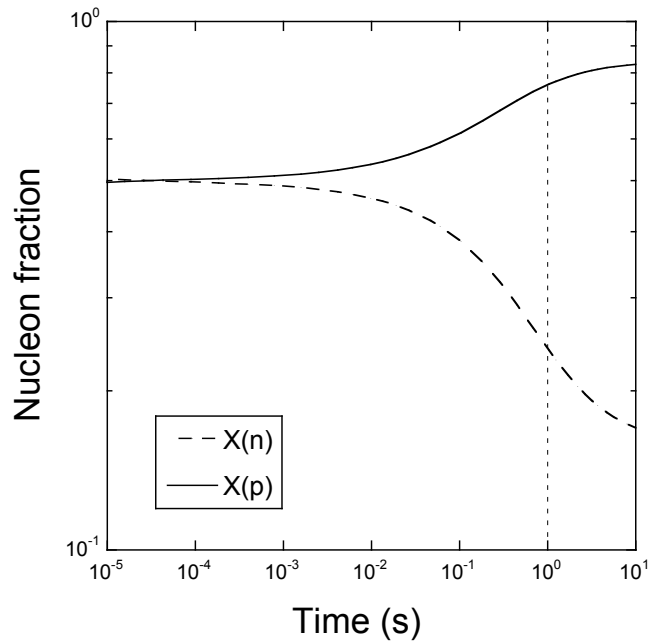


**Figure 2.** Nucleon fractions of protons (solid line) and neutrons (long-dashed line) for the first 10 s after the big bang. We start each reaction network calculation at time  $t = 1$  s after the big bang (vertical dashed line). Results are adopted from [Pitrou et al. \(2018\)](#).

*estimates of the simulated primordial abundances?* This question can best be answered using a Monte Carlo network technique ([Olive et al. 2000](#); [Nollett & Burles 2000](#); [Coc et al. 2002](#)). The following steps are involved. First, the rates of all 466 reactions in the network are randomly sampled (see below). Second, the network is numerically solved using this set of sampled rates. Third, the first two steps are repeated  $n$  times to collect an ensemble of final abundance yields;  $n$  must be sufficiently large for statistical fluctuations to become much smaller than the widths of the obtained abundance distributions. Fourth, final primordial abundances are extracted from the accumulated abundance probability densities.

The nuclear interaction rates are sampled using lognormal rate probability densities ([Coc et al. 2014](#); [Iliadis et al. 2015](#)). For a given reaction,  $j$ , and temperature,  $T$ , the rate probability density is expressed as

$$f[x(T)_j] = \frac{1}{\sigma\sqrt{2\pi}} \frac{1}{x(T)_j} e^{-[\ln x(T)_j - \mu(T)_j]^2 / [2\sigma(T)_j^2]} \quad (1)$$

where the lognormal parameters  $\mu$  and  $\sigma$  determine the location and the width of the distribution, respectively. For a lognormal probability density, rate samples,  $x_i$ , are drawn using ([Longland 2012](#))

$$x(T)_{ij} = x(T)_{med,j} [f.u.(T)]_j^{P(T)_{ij}} \quad (2)$$



where  $x_{med}$  and  $f.u.$  are the median rate value and the rate factor uncertainty, respectively. Both of these are listed in columns 2 and 3 of STARLIB, respectively. The quantity  $p_{ij}$  is a normally distributed random variable, i.e., it is given by a Gaussian distribution with an expectation value of zero and a standard deviation of unity. Note that  $f.u.(T)^{p(T)}$ , and not  $p(T)$ , is the factor by which the sampled reaction rate is modified compared to its median value. We will refer to  $p(T)$  as the *rate variation factor*.

We sample this rate variation factor for a given network run and nuclear reaction only once, i.e.,  $p(T)_{ij} = p_{ij}$  has the same value at all temperatures. This assumption was found to reproduce the abundance uncertainties arising from more complex sampling schemes (Longland 2012). It implies that the rate samples still depend on temperature, since Equation (2) takes the temperature dependence of the factor uncertainty,  $f.u.(T)$ , into account. Also, the rates of corresponding forward and reverse reactions are not sampled independently, because they are subject to the same value of the rate variation factor in a given network calculation.

The Monte Carlo procedure has major advantages compared to varying rates one-by-one in sequential network runs. It is straightforward to estimate primordial abundances by adopting the 16th, 50th, and 84th percentiles of the resulting abundance probability densities. The impact of a given reaction rate uncertainty on the nucleosynthesis can be quantified by storing the values of  $p_{ij}$  for each sample reaction network run. A scatter plot for the final abundance of a given nuclide versus the sampled value of  $p_{ij}$  can then be inspected for correlations. Below, we will present results obtained by computing 10,000 Monte Carlo reaction network samples.

Our simulated primordial abundances are listed in Table 3 and displayed in Figure 3, together with those obtained using the code PRIMAT (Pitrou et al. 2018) and the most recently published measured values.

The  $^4\text{He}$  abundance depends sensitively on the rates of the weak interactions,  $n \leftrightarrow p$ , for which we adopted the theoretical results of Pitrou et al. (2018) (see Table 1). The width of the abundance distribution, and, thus, the uncertainty of the predicted  $^4\text{He}$  abundance (Table 3), depends mainly on the experimental uncertainty of the neutron lifetime since this value was used to calibrate the theoretical weak interaction rates. Since we adopted the weak interaction rates of Pitrou et al. (2018), we do not obtain an improved value for the  $^4\text{He}$  nucleon fraction. Therefore, we do not list a present value of  $Y_p$  in Table 3.

For  $^2\text{H}$  (top panel in Figure 3), present and previous abundance predictions are in agreement. Interest-

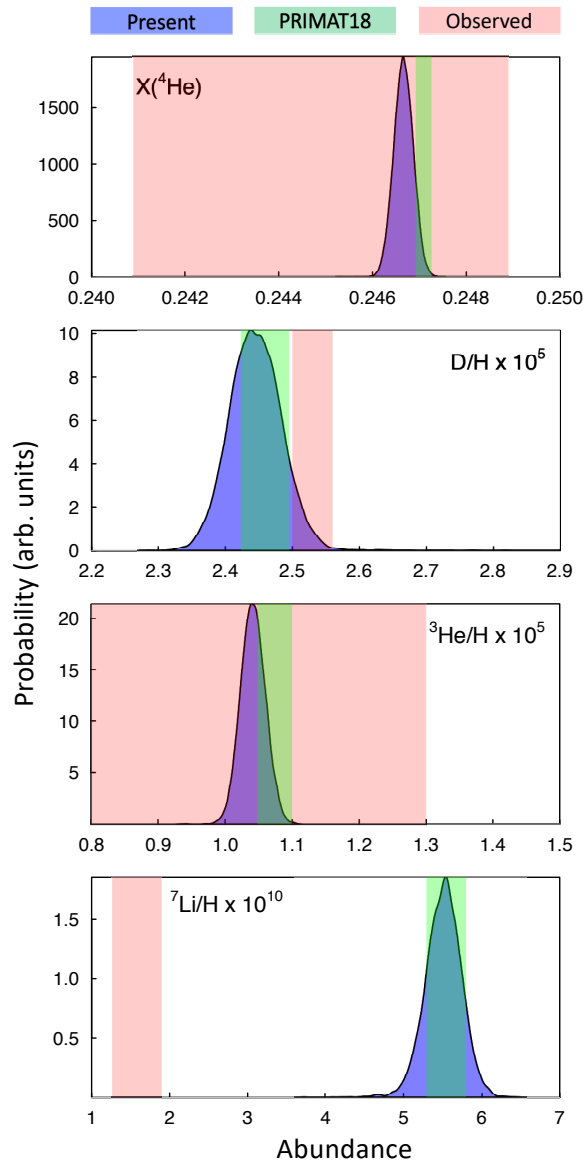


**Figure 3.** Number abundance ratios relative to  $^1\text{H}$  for primordial  $^2\text{H}$  (=D),  $^3\text{He}$ , and  $^7\text{Li}$ . (Blue) Simulated abundance probability densities from the present work. (Green) Simulated abundances reported by Pitrou et al. (2018). (Red) Observed values (see Table 3). The simulated results are based on 10,000 reaction network samples.

ingly, the measured value is larger by about 3% compared to the simulated ones. This “tension” had already been noted by Coc et al. (2015). The predicted deuterium abundance depends sensitively on the  $d(p,\gamma)^3\text{He}$  reaction rate for which we adopt the results of a recent Bayesian analysis (Table 1). New cross section data for

**Table 3.** Observed and predicted primordial abundances.<sup>a</sup>

	Observed <sup>b</sup>	Present <sup>c</sup>	PRIMAT18 <sup>d</sup>
$Y_p$	0.2449(40)	<sup>e</sup>	0.24709(17)
$(D/H)_p \times 10^{-5}$	2.527(30)	<b>2.445(37)</b>	2.459(36)
$(^3\text{He}/\text{H})_p \times 10^{-5}$	$\leq 1.1(2)$	<b>1.041(18)</b>	1.074(26)
$(^7\text{Li}/\text{H})_p \times 10^{-10}$	1.58(31)	<b>5.52(22)</b>	5.62(25)

<sup>a</sup>For  $^4\text{He}$ , the nucleon fraction ( $Y_p$ ) is given, while for the other species the number abundance ratio relative to  $^1\text{H}$  is listed. Uncertainties are given in parenthesis, e.g., “0.2449(40)” stands for “0.2449±0.0040.”

<sup>b</sup>From Aver et al. (2015); Cooke et al. (2018); Bania et al. (2002); Sbordone et al. (2010).

<sup>c</sup>Recommended values and uncertainties are obtained from the 16th, 50th, and 84th percentiles of the abundance probability densities (shaded blue in Figure 3).

<sup>d</sup>From Pitrou et al. (2018).

<sup>e</sup>No improvement was obtained in the present work compared to the  $Y_p$  value of Pitrou et al. (2018), see text.

this reaction are expected to be published soon by the LUNA collaboration<sup>3</sup>.

For  $^3\text{He}$  (middle panel in Figure 3), the simulated abundances agree with the observed upper limit (Bania et al. 2002). Our result is slightly lower than the simulation of Pitrou et al. (2018), which is explained by our adoption of the most recent  $^3\text{He}(d,p)\alpha$  rate (de Souza et al. 2019b) compared to their use of the older rate of Descouvemont et al. (2004).

Finally, the simulated present and previous  $^7\text{Li}$  abundance values (bottom panel in Figure 3) are in agreement, despite the fact that both studies employ different  $^7\text{Be}(n,p)^7\text{Li}$  reaction rates. The recent rate of de Souza et al. (2020), used here, has a significantly larger uncertainty than the rate of Descouvemont et al. (2004) that was used by Pitrou et al. (2018). Regardless, the simulated  $^7\text{Li}$  abundance exceeds the observed values by a factor of  $\approx 3$ , as has been pointed out before (Cyburt et al. 2003; Coc et al. 2004; Cuoco et al. 2004). We will consider correlations next.

## 5. CORRELATIONS BETWEEN ABUNDANCES AND REACTION RATES: MUTUAL INFORMATION

<sup>3</sup> The recent experimental cross sections of Tišma et al. (2019) have not yet been used in  $d(p,\gamma)^3\text{He}$  rate evaluations. The uncertainties of their four data points are larger than previous results.

We mentioned in Section 4 that the network Monte Carlo procedure lends itself to studying correlations between simulated abundances and reaction rates. Since final abundances and rate variation factors are stored after each network run, the analysis of correlation scatter plots will reveal the impact of the variation of each rate on the abundance of every nuclide in the network. The obvious challenge is to quantify which rates have the largest impact on a specific nuclide abundance. We need to adopt a useful metric to quantify the correlation, compute the metric for 50 isotopes  $\times$  466 reactions, and then sort the results according to impact. Pearson’s (product-moment correlation coefficient)  $r$ , which was used by Coc et al. (2014), is a measure for the linear correlation between two random variables. Iliadis et al. (2015) suggested to use Spearman’s (rank-order correlation coefficient)  $r_s$ , which quantifies how well the relationship between two variables is described by a monotonic function. However, these metrics are not without problems in the present context, where correlations are frequently neither linear nor monotonic.

Here, we will adopt the *mutual information* metric, which originates from information theory (Linfoot 1957; Cover & Thomas 2006). It quantifies how much information is communicated, on average, in one random variable about another when both are sampled simultaneously. For two random variables,  $Y$  and  $Z$ , with values of  $\{y_1, y_2, y_3, \dots\}$  and  $\{z_1, z_2, z_3, \dots\}$ , respectively, their mutual information is defined by

$$MI = \sum_y \sum_z P(y, z) \log \left[ \frac{P(y, z)}{P(y)P(z)} \right] \quad (3)$$

where  $P(y)$  and  $P(z)$  are marginal distributions of  $y$  and  $z$ , respectively, and  $P(y, z)$  is the joint probability density. An important theorem from information theory states that the mutual information between two variables is zero if, and only if, the two random variables are statistically independent. Unlike Pearson’s  $r$  and Spearman’s  $r_s$  coefficients, mutual information has no finite upper bound and, therefore, its absolute magnitude has no straightforward interpretation. However, here we are mainly interested in identifying the most important reactions for a given nuclide. For this purpose, the relative magnitude of the mutual information will suffice<sup>4</sup>.

<sup>4</sup> Linfoot (1957) suggested to transform the mutual information by introducing the *informational coefficient of correlation*, defined as  $IC \equiv \sqrt{1 - e^{-2 \cdot MI}}$ . The coefficient  $IC$  lies between 0 and 1, equals zero when the two random variables are statistically independent, and equals unity when they are fully correlated. Again, there is no need in the present work to normalize the mutual information,  $MI$ .

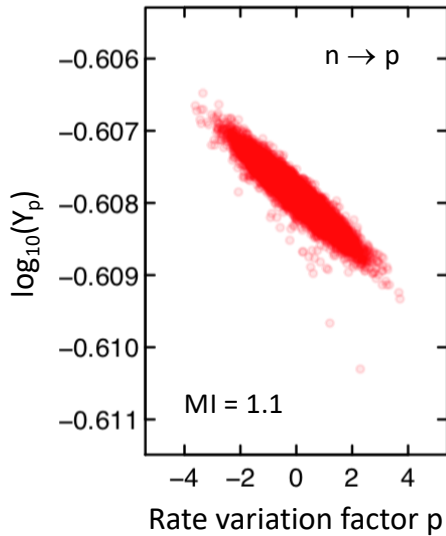


**Figure 4.** Correlation of the simulated primordial  ${}^4\text{He}$  abundance with the rate variation factor of the weak interactions that transform neutrons into protons (Section 3). The value for the mutual information correlation metric is also given ( $\text{MI} = 1.1$ ). The  ${}^4\text{He}$  abundance exhibits no noticeable correlation with any other reaction in the network, given the rate uncertainties adopted here. The results are obtained for the same simulations that gave rise to Figure 3.

### 5.1. ${}^4\text{He}$ abundance

The weak interactions,  $n \leftrightarrow p$ , have the largest impact on the primordial  ${}^4\text{He}$  abundance (Section 3). The correlation between  $Y_p$  and the rate variation factor for  $n \rightarrow p$  is presented in Figure 4. The mutual information amounts to a value of  $\text{MI} = 1.1$ . None of the other reactions in the network are noticeably correlated with  $Y_p$ , i.e., all other mutual information values are  $\text{MI} \leq 0.02$ . As already noted in Section 2, the weak interaction rate uncertainty is given by the present uncertainty in the neutron decay constant.

Interestingly, if one would assume a factor of 10 uncertainty for the  $d(n,\gamma)t$  rate, the  ${}^4\text{He}$  abundance distribution would display a pronounced tail on the right side of the peak. The published rate uncertainty (Nagai et al. 2006) for this reaction is only 8%, although it is not clear to us how this value was derived. In the present work, we adopt a conservative uncertainty of a factor of 2. With this assumption, the  $d(n,\gamma)t$  reaction rate uncertainty has only a negligible impact on the primordial  ${}^4\text{He}$  abundance. More information about the experiment of Nagai et al. (2006) is given in Appendix A.1.

### 5.2. ${}^2\text{H}$ abundance

The primordial deuterium abundance is mainly impacted by the rate uncertainties of the  $d(p,\gamma){}^3\text{He}$ ,

$d(d,n){}^3\text{He}$ , and  $d(d,p)t$  reactions. The correlations are depicted in Figure 5. The  $d(p,\gamma){}^3\text{He}$  reaction is by far the most important among the three processes, as can be seen from its much larger mutual information value ( $\text{MI} = 0.59$ ) compared to the  $d(d,n){}^3\text{He}$  ( $\text{MI} = 0.09$ ) and  $d(d,p)t$  ( $\text{MI} = 0.07$ ) reactions. The rate uncertainties are listed in Table 1 and have been derived using Bayesian techniques for all three reactions.

As expected, the  $d(p,\gamma){}^3\text{He}$  rate is negatively correlated with the deuterium abundance: a smaller rate will result in a larger abundance of surviving deuterium nuclei. The present rate uncertainty for the  $d(p,\gamma){}^3\text{He}$  reaction is 3.7%. Decreasing the recommended rate by 9% would shift the centroid of the simulated deuterium abundance distribution into the center of the observed range (top panel in Figure 3). Clearly, a new and improved measurement of the  $d(p,\gamma){}^3\text{He}$  reaction is of significant interest (see Section 3).

Figure 5 also displays the correlation for the  ${}^3\text{He}(t,d)\alpha$  reaction ( $\text{MI} = 0.04$ ). The vast majority of network samples reveals an uncorrelated  ${}^2\text{H}$  abundance, as can be seen from a distribution of points that is symmetric about a rate variation factor of  $p = 0$ . However, a few samples, for large values of  $p$ , do reveal a correlation. For this reaction, we adopted a rate uncertainty factor of  $f.u. = 10$ . An arbitrary increase of the recommended rate by a factor of 400 would also shift the peak of the simulated deuterium abundance distribution into the center of the observed range. The status of the rate of this reaction is discussed in Appendix A.2.

### 5.3. ${}^3\text{He}$ abundance

The primordial  ${}^3\text{He}$  abundance is mainly influenced by the two reactions that produce and destroy  ${}^3\text{He}$ ,  $d(p,\gamma){}^3\text{He}$  and  ${}^3\text{He}(d,p)\alpha$ , respectively. Correlations can be found in Figure 6. The mutual information values are  $\text{MI} = 0.58$  and  $\text{MI} = 0.14$ , respectively, for these two reactions. The reaction rate uncertainties are listed in Table 1 and have been derived using Bayesian techniques. None of the other reactions in the network are noticeably correlated with the  ${}^3\text{He}$  abundance, i.e., all other mutual information values are  $\text{MI} \leq 0.02$ .

### 5.4. ${}^7\text{Li}$ abundance

Of the primordial lithium synthesized in the early universe, about 95% originated from radioactive  ${}^7\text{Be}$  during primordial nucleosynthesis, which later decayed to  ${}^7\text{Li}$  when the expansion of the universe gave rise to temperatures and densities insufficient to sustain nuclear reactions. The final  ${}^7\text{Li}$  abundance is mainly impacted by the rate uncertainties of the  ${}^3\text{He}(\alpha,\gamma){}^7\text{Be}$ ,  $d(p,\gamma){}^3\text{He}$ ,  ${}^7\text{Be}(d,p)2\alpha$ , and  ${}^7\text{Be}(n,p){}^7\text{Li}$  reactions. The correlations



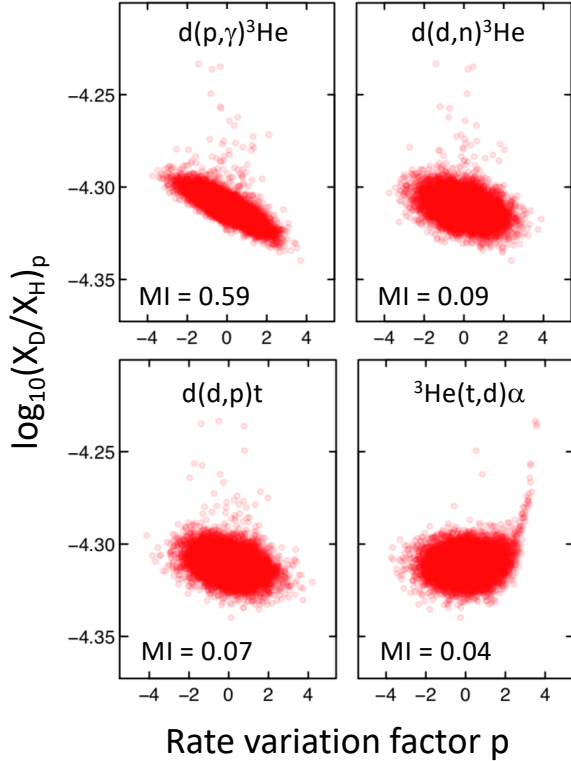


**Figure 5.** Correlation of the simulated primordial deuterium-to-hydrogen ratio with the rate variation factors of the reactions  $d(p,\gamma)^3\text{He}$ ,  $d(d,n)^3\text{He}$ ,  $d(d,p)t$ , and  $^3\text{He}(t,d)\alpha$ . The values for the mutual information (MI) are also given. The rate uncertainties of all other reactions in the network have a negligible impact on this abundance ratio. The results are obtained for the same simulations that gave rise to Figure 3. The ordinate shows the logarithm of the mass fraction ratio instead of the number abundance ratio.

are provided in Figure 7. The mutual information values for these four reactions amount to  $\text{MI} = 0.20, 0.19, 0.11,$  and  $0.07$ , respectively. The mutual information values of all other reactions in the network are  $\text{MI} \leq 0.03$ .

Recently estimated Bayesian rates are available for the  $^3\text{He}(\alpha,\gamma)^7\text{Be}$ ,  $d(p,\gamma)^3\text{He}$ , and  $^7\text{Be}(n,p)^7\text{Li}$  reactions (see Table 1). A more recent  $^3\text{He}(\alpha,\gamma)^7\text{Be}$  rate has been published by Singh et al. (2019), which is based on the calculation of Dubovichenko et al. (2018). However, these results are highly problematic and should not be used in big bang nucleosynthesis simulations, for reasons explained in Appendix A.3. The status of the  $d(p,\gamma)^3\text{He}$  reaction rate has already been mentioned in connection with the primordial deuterium abundance (Section 5.2). The uncertainty of the most recently published  $^7\text{Be}(n,p)^7\text{Li}$  rate (de Souza et al. 2020) is 2.1% at big bang nucleosynthesis temperatures (Table 1).

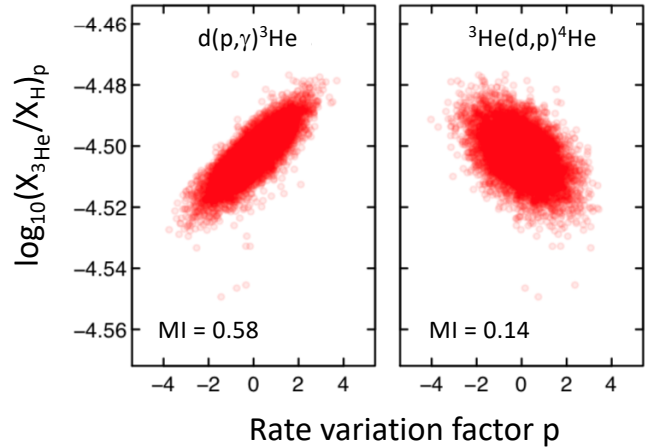


**Figure 6.** Correlation of the simulated primordial  $^3\text{He}$ -to-hydrogen ratio with the rate variation factors of the reactions  $d(p,\gamma)^3\text{He}$  and  $^3\text{He}(d,p)\alpha$ . The values for the mutual information (MI) are also given. The rate uncertainties of all other reactions in the network have a negligible impact on the abundance ratio. The results are obtained for the same simulations that gave rise to Figure 3. The ordinate shows the logarithm of the mass fraction ratio instead of the number abundance ratio.

Figure 7 indicates a noticeable tail towards smaller primordial  $^7\text{Li}$  abundances for large values of the  $^7\text{Be}(d,p)2\alpha$  reaction rate variation factor,  $p$ . In our simulations, we adopted the recently published rate of Rijal et al. (2019a), which has a reported uncertainty of a factor of  $\approx 3$  at big bang nucleosynthesis temperatures. Increasing the recommended rate by a factor of  $\gtrsim 200$  would lead to a significant overlap between the predicted and measured abundance values, and, thus, would solve the cosmological lithium problem. Considering the large uncertainties involved in the experiment of Rijal et al. (2019a) (30% in the absolute cross section normalization and  $\pm 45$  keV in the experimental energy calibration), it is important to remeasure this reaction in the future with improved techniques. More information regarding the present status of the  $^7\text{Be}(d,p)2\alpha$  reaction is provided in Appendix A.4.

## 6. UNKNOWN SYSTEMATIC BIAS IN REACTION RATES: GENETIC ALGORITHM

In Section 4, we discussed how to estimate primordial abundances, given a set of thermonuclear rates for the key nuclear reactions (Table 1) that were derived from measured data, by taking into account all known statistical and systematic effects. In agreement with previous work, we find that the simulated primordial lithium abundance exceeds the measured value by a factor of  $\approx 3$  (Section 4). However, suppose that one or more nuclear reaction rates are subject to some unknown systematic

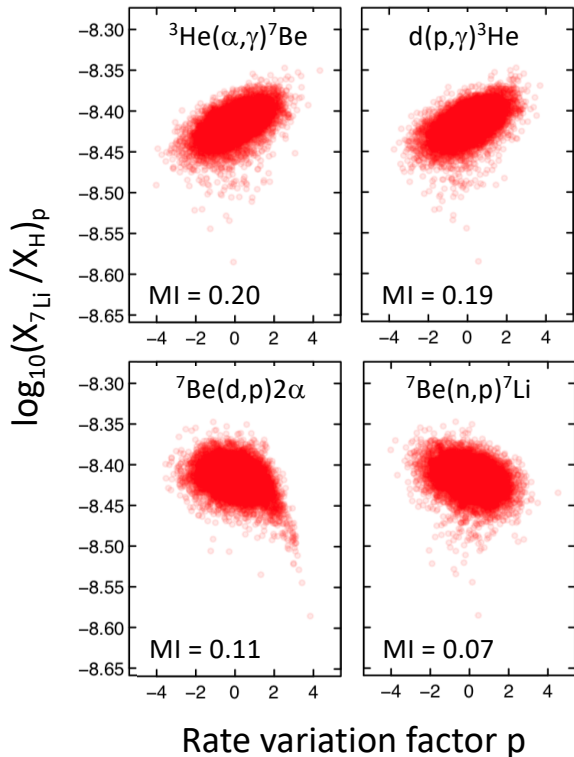


**Figure 7.** Correlation of the simulated primordial  ${}^7\text{Li}$ -to-hydrogen ratio with the rate variation factors of the reactions  ${}^3\text{He}(\alpha,\gamma){}^7\text{Be}$ ,  $d(p,\gamma){}^3\text{He}$ ,  ${}^7\text{Be}(d,p)2\alpha$ , and  ${}^7\text{Be}(n,p){}^7\text{Li}$ . The values for the mutual information (MI) are also given. The rate uncertainties of all other reactions in the network have a negligible impact on the abundance ratio. The results are obtained for the same simulations that gave rise to Figure 3. The ordinate shows the logarithm of the mass fraction ratio instead of the number abundance ratio.

bias, so that their true magnitudes differ significantly from the reported values. Therefore, in this section we ask a different question: *By what factors would one need to multiply key reaction rates to reproduce simultaneously all observed primordial abundances?*

The answer to this question is not simply obtained by independently changing the rates of individual nuclear reactions. We already discussed in Section 5 that, for example, the  $d(p,\gamma){}^3\text{He}$  reaction impacts the primordial abundances of  ${}^2\text{H}$ ,  ${}^3\text{He}$ , and  ${}^7\text{Li}$  (Figures 5, 6, and 7, respectively). Therefore, we must consider the simultaneous rate changes of several nuclear reactions.

We will focus on the reactions  $d(p,\gamma){}^3\text{He}$ ,  ${}^3\text{He}(\alpha,\gamma){}^7\text{Be}$ ,  ${}^7\text{Be}(d,p)2\alpha$ , and  ${}^7\text{Be}(n,p){}^7\text{Li}$ , which correlate most strongly with the primordial  ${}^7\text{Li}$  abundance (Figure 7). We require that simultaneous rate changes of these reactions reproduce the measured  ${}^2\text{H}$ ,  ${}^3\text{He}$ , and  ${}^7\text{Li}$  abundances (Table 3). Although Bania et al. (2002) prefer to report an upper limit for the  ${}^3\text{He}$  abundance inferred

from their observations of distant metal-poor galactic H II regions, their upper limit value agrees with the simulated primordial  ${}^3\text{He}$  abundance (Table 3). Therefore, for the discussion in this section, we will follow the suggestion of Steigman (2007) and adopt the upper limit of Bania et al. (2002) as an estimate of the primordial  ${}^3\text{He}$  abundance.

To investigate this optimization problem, we use a genetic algorithm, which provides a robust means of finding the global extremum in a multi-dimensional parameter space. Genetic algorithms are inspired by the mechanism of biological evolution through natural selection. See, for example, Goldberg (1989) for details. In brief, the idea is to start with an initial population of unbiased random sets of model parameter values. Each such set represents an individual in the overall population. Depending on their fitness, pairs of individuals are selected for the operations of crossover and mutation to produce offspring until the current generation of individuals has been replaced by a new generation of offsprings. The fitness of each offspring is assessed, and the process repeats itself by evolving through subsequent generations. As a result, the average population fitness increases over time, i.e., a better solution is produced with each generation. The process is terminated when a suitable solution (e.g., a parameter set of predefined fitness) is found or a given number of generations is reached. A major benefit of genetic algorithms is their ability to explore different parts of parameter space simultaneously (Holland 1992).

For the genetic algorithm-based optimizer, we used the general-purpose subroutine PIKAIA v1.2<sup>5</sup>, which was first presented in Charbonneau (1995); Gibson & Charbonneau (1998). It uses a stochastic rank-based selection scheme, a uniform one-point crossover (occurring with a probability of 0.85), and a uniform one-point adjustable mutation rate based on fitness. We set the initial, minimum, and maximum mutation probabilities to values of 0.005, 0.0005, and 0.25, respectively. For the reproduction plan, we chose the “steady-state-deleto-worst” option, where the least fit individual of the parent population is eliminated and replaced by the offspring.

Fitness is the only point of contact between the genetic algorithm and the problem being solved. We will adopt a figure of merit of the form

$$\chi^2(\mathbf{u}) = \sum_{i=1}^3 \frac{[y_{obs,i} - y_i(\mathbf{u})]^2}{\sigma_{obs,i}^2} \quad (4)$$

<sup>5</sup> The public domain source code and accompanying documentation is available at <https://www.hao.ucar.edu/modeling/pikaia/pikaia.php>.

where  $y_i$  and  $\sigma_i$  denote the mean values and uncertainties, respectively, of the  $^2\text{H}$ ,  $^3\text{He}$ , and  $^7\text{Li}$  measured abundances (Table 3), and  $y_i(\mathbf{u})$  are the corresponding predictions that depend on the vector of model parameters,  $\mathbf{u}$ . In our context, the model parameters,  $u_1$ ,  $u_2$ ,  $u_3$ , and  $u_4$ , are the rate multiplication factors of the reactions  $\text{d}(\text{p},\gamma)^3\text{He}$ ,  $^3\text{He}(\alpha,\gamma)^7\text{Be}$ ,  $^7\text{Be}(\text{d},\text{p})2\alpha$ , and  $^7\text{Be}(\text{n},\text{p})^7\text{Li}$ , respectively. The fitness can then be defined as  $f = \chi^{-2}$ . If the predictions for all three abundances,  $(\text{D}/\text{H})_p$ ,  $(^3\text{He}/\text{H})_p$ , and  $(^7\text{Li}/\text{H})_p$ , agree with their respective observations within uncertainties, then  $f \gtrsim 0.33$  according to Equation (4).

First, we restricted the search to the parameter regions  $0.9 < u_1 \leq 1.1$ ,  $0.9 < u_2 \leq 1.1$ ,  $0.033 < u_3 \leq 30$ ,  $0.5 < u_4 \leq 2$ . These ranges significantly exceed the reported rate uncertainties listed in column 2 of Tables 1 and 1. The result of the evolutionary run is shown in Figure 8. The top panel displays the value of  $f$  for the fittest individual in each generation. The system is seen to converge after  $\approx 100$  generations. After 1000 generations, the maximum fitness value found by the algorithm was only  $f = 0.11$ . In other words, changing the rates of these four reactions within the ranges specified above cannot reproduce the observational abundances. The bottom panel presents the corresponding evolution of the rate multiplication factors. While the factors for  $\text{d}(\text{p},\gamma)^3\text{He}$  and  $^3\text{He}(\alpha,\gamma)^7\text{Be}$  are near unity ( $u_1 \approx u_2 \approx 1$ ), those for  $^7\text{Be}(\text{d},\text{p})2\alpha$  and  $^7\text{Be}(\text{n},\text{p})^7\text{Li}$  are at the upper values of their search ranges ( $u_3 \approx 30$ ,  $u_4 \approx 2$ ). Similar results are obtained with different random number seeds.

Since the  $^4\text{He}$  nucleon fraction depends mainly on the weak interaction rates, we have three data points (observations of  $^2\text{H}$ ,  $^3\text{He}$ , and  $^7\text{Li}$ ) and four parameters (reaction rate multiplication factors). Because our system is underdetermined, we expect, in general, more than one possible combination of parameter values that could reproduce the observations, depending on the constraints (parameter ranges) applied. However, the important point is that the genetic algorithm does not find any acceptable solution at all if the rates of key reactions are varied simultaneously over ranges that are large compared to the reported uncertainties.

Once the search ranges for  $^7\text{Be}(\text{d},\text{p})2\alpha$  and  $^7\text{Be}(\text{n},\text{p})^7\text{Li}$  ( $u_3$  and  $u_4$ , respectively) are widened even more, the genetic algorithm finds, within only a few generations, many different acceptable solutions ( $f \gtrsim 0.33$ ), depending on the magnitude of the search ranges. For example, agreement between observed and simulated abundances is achieved if the  $^7\text{Be}(\text{d},\text{p})2\alpha$  and  $^7\text{Be}(\text{n},\text{p})^7\text{Li}$  rates are simultaneously multiplied by factors of  $u_3 \approx 0.2$  and  $u_4 \approx 3.4$ , respectively, or if the  $^7\text{Be}(\text{d},\text{p})2\alpha$  and  $^7\text{Be}(\text{n},\text{p})^7\text{Li}$  rates alone are multiplied by factors of  $u_3 \approx 410$  and  $u_4$

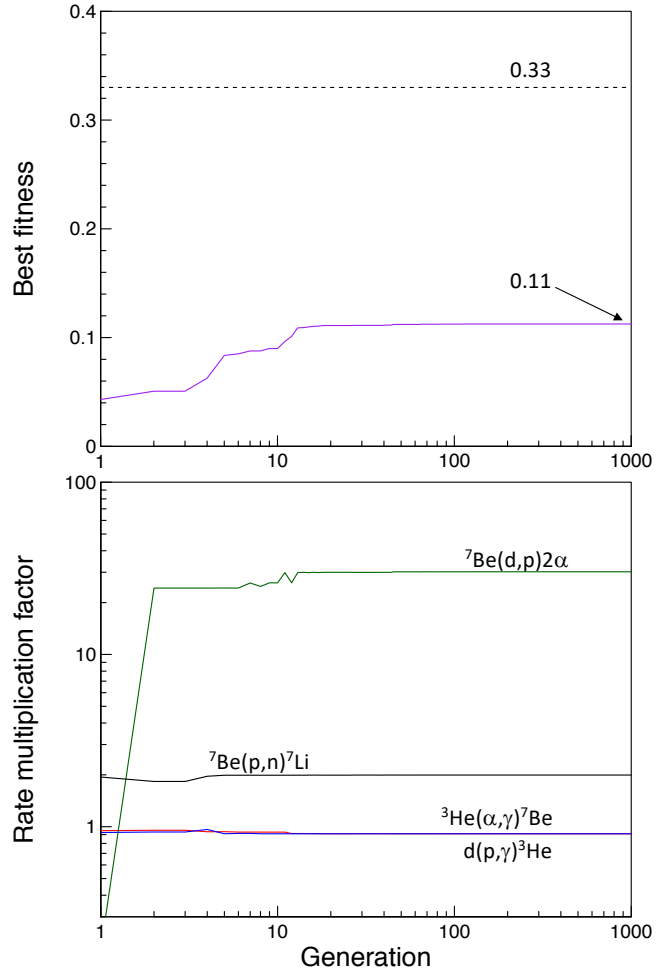


**Figure 8.** Application of a genetic algorithm to search for possible reaction rate changes that could account for the measured primordial abundances,  $(\text{D}/\text{H})_p$ ,  $(^3\text{He}/\text{H})_p$ , and  $(^7\text{Li}/\text{H})_p$ . The simultaneous rate changes considered are those for the  $\text{d}(\text{p},\gamma)^3\text{He}$ ,  $^3\text{He}(\alpha,\gamma)^7\text{Be}$ ,  $^7\text{Be}(\text{d},\text{p})2\alpha$ , and  $^7\text{Be}(\text{n},\text{p})^7\text{Li}$  reactions. The search ranges for these rates significantly exceed the magnitude of their reported uncertainties (see text). (Top) Evolution of best fitness in each generation. The dashed line ( $f = 0.33$ ) indicates the fitness for which the predicted and measured primordial abundances of  $^2\text{H}$ ,  $^3\text{He}$ , and  $^7\text{Li}$  would be in agreement. (Bottom) Corresponding evolution of the reaction rate multiplication factors. No acceptable solution ( $f \gtrsim 0.33$ ) is found after 1000 generations. The population size was 100.

$\approx 4.0$ , respectively. Based on the current status of the nuclear physics data, we find such large rate changes to be unlikely. For more information about the  $^7\text{Be}(\text{d},\text{p})2\alpha$  reaction, see Appendix A.4.

## 7. CONCLUDING SUMMARY

This work focused on a discussion of thermonuclear reaction rates for big bang nucleosynthesis simulations. We started by summarizing the most recently pub-

lished reaction rates. Among the twelve nuclear processes that are key to primordial element synthesis, the rates of seven reactions,  $d(p,\gamma)^3\text{He}$ ,  $d(d,p)t$ ,  $d(d,n)^3\text{He}$ ,  $^3\text{He}(d,p)\alpha$ ,  $t(d,n)\alpha$ ,  $^3\text{He}(\alpha,\gamma)^7\text{Be}$ , and  $^7\text{Be}(n,p)^7\text{Li}$ , have been analyzed using Bayesian techniques (Table 1). Such methods provide results that are less biased when compared to previously applied techniques. Subsequently, we discussed other input to our reaction network, such as the evolution of temperature and density in the early universe, and initial abundances. We then presented simulated primordial abundances,  $(D/H)_p$ ,  $(^3\text{He}/H)_p$ , and  $(^7\text{Li}/H)_p$ , including their uncertainties. These were obtained using a reaction network Monte Carlo method, i.e., by simultaneously sampling the rates of all reactions in our network according to their rate probability densities. In agreement with previous works, our simulated  $^7\text{Li}$  abundance exceeds the measured primordial value by a factor of  $\approx 3$ . Correlations between predicted abundances and reaction rates were analyzed using the metric of mutual information, which originates from information theory. The most important reactions for the synthesis of  $^7\text{Li}$  are, in decreasing order, ac-

ording to their mutual information values,  $d(p,\gamma)^3\text{He}$ ,  $^3\text{He}(\alpha,\gamma)^7\text{Be}$ ,  $^7\text{Be}(d,p)2\alpha$ , and  $^7\text{Be}(n,p)^7\text{Li}$ . These conclusions are based on thermonuclear rates that were derived by taking into account all known statistical and systematic effects in the data analysis. Finally, for these four reactions, we account for *unknown* systematic bias in the data by using a genetic algorithm to search for rate multiplication factors that would reconcile all simulated and measured primordial abundances. No such solutions were found within reasonable search ranges, adding weight to previous findings that the solution of the cosmological lithium problem is unlikely to be found within the realm of nuclear physics.

We would like to thank Rafael S. de Souza for his help with the genetic algorithm. We would also like to express our gratitude to Robert Janssens for providing valuable feedback. This work was supported in part by NASA under the Astrophysics Theory Program grant 14-ATP14-0007 and by U.S. DOE under contracts DE-FG02-97ER41041 (UNC) and DE-FG02-97ER41033 (TUNL).

## APPENDIX

### A. COMMENTS ON SPECIFIC NUCLEAR REACTIONS

#### A.1. $d(n,\gamma)t$

The  $d(n,\gamma)t$  has been measured by Nagai et al. (2006) in the energy range important for primordial nucleosynthesis. Their three measured cross section data points, at neutron energies of 30.5 keV, 54.2 keV, and 521 keV, have uncertainties between 10% and 15%, including counting statistics, detector response, correction factors, and absolute normalizations. Their data, including previous results of thermal-neutron capture measurements (Jurney et al. 1982), were fit using a theoretical calculation based on the Faddeev approach. However, Nagai et al. (2006) provide insufficient information to assess how this input translates to a reaction rate uncertainty of only 8%. For the present simulations, we adopted a more conservative rate factor uncertainty of  $f.u. = 2$ .

#### A.2. $^3\text{He}(t,d)\alpha$

The  $^3\text{He}(t,d)\alpha$  recommended rate used in the present work was adopted from Caughlan & Fowler (1988). This rate is presumably the same as the one published in Fowler et al. (1967), who quote as reference Youn et al. (1961). The latter work measured the  $^3\text{He} + t$  cross section at triton energies in the range from 150 to 970 keV. Their result is in reasonable agreement with Smith et al. (1963), who measured the cross section at a higher triton

energy of 1.9 MeV, but disagrees with the earlier measurement of Moak (1953), who obtained a cross section higher by a factor of  $\approx 3$ . Fowler et al. (1967) assigned a rate uncertainty of  $\pm 30\%$  to the  $^3\text{He}(t,d)\alpha$  reaction at all temperatures below  $T \leq 10$  GK. Although the data are sparse and exhibit significant inconsistencies, it is unlikely that this rate could change by a factor of  $\approx 400$  required to impact the primordial deuterium abundance significantly, as discussed in Section 5.2. In the present work, we adopted a conservative uncertainty of a factor 10 for this rate.

#### A.3. The $^3\text{He}(\alpha,\gamma)^7\text{Be}$ rate

For a long time, measurements of the  $^3\text{He}(\alpha,\gamma)^7\text{Be}$  reaction have been plagued by systematic effects. Depending on the detection geometry, either the prompt  $\gamma$  rays, the  $^7\text{Be}$  decay, or the recoiling  $^7\text{Be}$  nuclei were detected. However, the cross section data from different measurements displayed significant differences. Consequently, the reaction rate based on the available data was rather uncertain (Angulo et al. 1999; Descouvemont et al. 2004). The situation at the time called for new, careful measurements. The S-factors measured subsequently (Nara Singh et al. 2004; Brown et al. 2007; di Leva et al. 2009; Costantini et al. 2008), which are displayed in Figure 9 as black data points, are in overall agreement. Also, some groups have applied all three different experimental methods (prompt, decay, and recoil



detection), yielding consistent results. Compared to the older measurements (see, for example, Figure 3 of Neff (2011)), the modern data are systematically higher and have a significantly smaller dispersion.

These modern  ${}^3\text{He}(\alpha,\gamma){}^7\text{Be}$  data were used in a number of studies to derive reaction rates (Cyburt & Davids 2008; Adelberger et al. 2011; Iliadis et al. 2016). The solid black line in Figure 9 displays the fit based on a hierarchical Bayesian model (Iliadis et al. 2016). It resulted in a reaction rate with an uncertainty of 2.4% in the temperature range of big bang nucleosynthesis (Table 1). This rate was adopted in the present work.

Unfortunately, recent publications (Dubovichenko et al. 2018, 2019; Singh et al. 2017) have led to confusing claims that cannot be substantiated, as will be explained below. The fit of Iliadis et al. (2016) did not take into account the single data point of Takács et al. (2018), who inferred the  ${}^3\text{He}(\alpha,\gamma){}^7\text{Be}$  S-factor at solar energy from the solar neutrino flux. This indirect determination is not on par with the direct measurements mentioned above because it is difficult to assess the systematic uncertainties involved. This data point, shown in green in Figure 9, reveals large uncertainties and is located far away from the energy range important to primordial nucleosynthesis. However, motivated by this result, a new theoretical S-factor for the  ${}^3\text{He}(\alpha,\gamma){}^7\text{Be}$  reaction has been proposed by Dubovichenko et al. (2018, 2019), which is shown as the dashed blue line. It can be seen that the fit of Iliadis et al. (2016) (and those of Cyburt & Davids (2008); Adelberger et al. (2011)) and the theoretical prediction of Dubovichenko et al. (2018, 2019) both agree with the (green) data point at solar energy. However, importantly, the theoretical S-factor of Dubovichenko et al. (2018, 2019) clearly disagrees with all of the modern data at the energies most relevant for big bang nucleosynthesis. In conclusion, the S-factor of Dubovichenko et al. (2019) should not be used in primordial nucleosynthesis calculations. It underpredicts the data by about 15%, implying a reduction in the simulated primordial lithium abundance by a similar amount.

The reason why we have discussed the results of Dubovichenko et al. (2018, 2019) in some detail is because their S-factor was adopted in the big bang nucleosynthesis simulations of Singh et al. (2017). The latter authors reported a smaller predicted lithium abundance,  $({}^7\text{Li}/\text{H})_p = (4.447 \pm 0.067) \times 10^{-10}$ , which appears to be in lesser disagreement with the observed value (Table 3). However, as explained above, their result is erroneous because it rests on an inappropriate S-factor extrapolation from the solar region to the energy range of primordial nucleosynthesis.

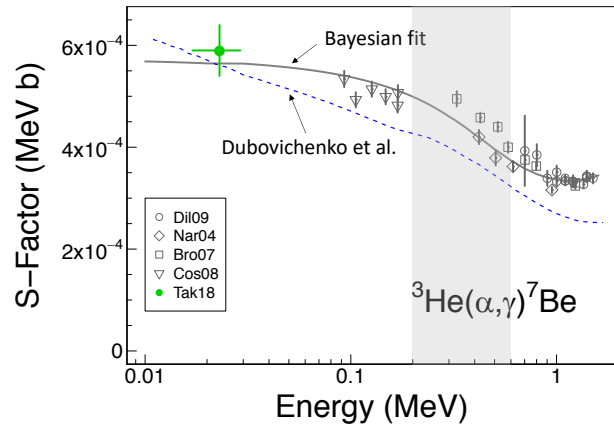


**Figure 9.** Measured and predicted  ${}^3\text{He}(\alpha,\gamma){}^7\text{Be}$  S-factors. The modern (published after 2000) data for the direct measurement are shown in black: Dii09 (di Leva et al. 2009), Bro07 (Brown et al. 2007), Nar04 (Nara Singh et al. 2004), Cos08 (Costantini et al. 2008). The green data point depicts the value obtained indirectly by Takács et al. (2018). The black solid line corresponds to the Bayesian fit of Iliadis et al. (2016), which is close to the fits (not shown) of Cyburt & Davids (2008) and Adelberger et al. (2011). The dashed blue line indicates the theoretical prediction of Dubovichenko et al. (2018, 2019), which is clearly incompatible with the data shown at energies important for primordial  ${}^7\text{Be}$  synthesis (shaded region).

#### A.4. The ${}^7\text{Be}(d,p)2\alpha$ rate

The  ${}^7\text{Be}(d,p)2\alpha$  reaction was recognized for some time as the most promising one for solving the cosmological lithium problem (Coc et al. 2004). Its rate required an increase by about two orders of magnitude compared to the rate of Caughlan & Fowler (1988) to significantly reduce the  ${}^7\text{Li}$  yield; see Figure 4 in Coc et al. (2004) and Table I in Coc et al. (2012). The Caughlan & Fowler (1988) rate was adopted from Parker (1972), who assumed a constant S-factor of 100 MeVb based on the experimental data of Kavanagh (1960). Parker (1972) writes: “*Experimental measurements of the differential cross-section for this reaction were made by Kavanagh (1960) for deuteron energies from 700 to 1700 keV. Lacking complete angular distributions, these data can be approximately converted to total cross sections by multiplying by  $4\pi$  and (2) by multiplying by a factor of 3 to take into account contributions from higher excited states in  ${}^8\text{Be}$ .*” Unobserved resonances that could significantly increase the cross section were proposed by Chakraborty et al. (2011); Brogini et al. (2012). Until very recently, this possibility seemed unlikely based on measurements of the average cross section (Angulo et al. 2005) and investigations of the properties of candidate resonances (O’Malley et al. 2011; Scholl et al. 2011; Kirsebom & Davids 2011). Notice that the exper-



iment by [Angulo et al. \(2005\)](#) was only sensitive to the  ${}^7\text{Be}(\text{d,p}){}^8\text{Be}(2\alpha)$  reaction channel.

In a recent experiment, [Rijal et al. \(2019a\)](#); [Rijal et al. \(2019b\)](#) found a new resonance in the previously undetected  ${}^7\text{Be}(\text{d},\alpha){}^5\text{Li}(\text{p}\alpha)$  channel. Their experimental S-factor is much higher compared to the results of [Kavanagh \(1960\)](#) and [Angulo et al. \(2005\)](#). This conclusion was supported by preliminary results of [Inoue et al. \(2018\)](#), showing an increase of the S-factor around  $E_{\text{cm}} \approx 0.3$  MeV.

Although the experiment by [Rijal et al. \(2019a\)](#) provided valuable data at temperatures relevant to primordial nucleosynthesis, the magnitude of the reaction rates in the temperature range of primordial nucleosynthesis changed only modestly compared to earlier estimates. [Pitrou et al. \(2019\)](#); [Gai \(2019\)](#); [Coc & Davids \(2019\)](#) pointed out that the recommended rate of [Rijal et al. \(2019a\)](#) is close to the result of [Parker \(1972\)](#); [Caughlan & Fowler \(1988\)](#), who had introduced an approximate

rate multiplication factor of 3. Also, the rate uncertainty reported in [Rijal et al. \(2019a\)](#) is close to the factor of 3 uncertainty adopted by [Pitrou et al. \(2018\)](#). Figure 10 displays the rates of [Rijal et al. \(2019a\)](#) as blue lines and those adopted by [Pitrou et al. \(2018\)](#) as red lines. The shaded region indicates the relevant temperature range. The rate difference is much smaller than the two orders of magnitude required for a significant change in the predicted primordial lithium abundance; see Table 3 and [Pitrou et al. \(2019\)](#); [Fields et al. \(2020\)](#); [Coc & Davids \(2019\)](#). We also note that the claim in [Rijal et al. \(2019b\)](#) of a  $\approx 5\%$  reduction in the primordial lithium abundance when the  ${}^7\text{Be}(\text{d,p})2\alpha$  rate is set equal to zero is most likely erroneous. In our network calculations, the reduction amounts to only 0.75%.

It is, nevertheless, of interest to remeasure the  ${}^7\text{Be}(\text{d,p})2\alpha$  reaction and to reduce the uncertainties in resonance energy and cross section, as suggested by [Rijal et al. \(2019a\)](#).

## REFERENCES

- Adelberger, E. G., García, A., Robertson, R. G. H., et al. 2011, *Rev. Mod. Phys.*, 83, 195
- Aghanim, N., Akrami, Y., Ashdown, M., et al. 2018, Planck 2018 results. VI. Cosmological parameters, , , arXiv:1807.06209
- Aguado, D. S., González Hernández, J. I., Allende Prieto, C., & Rebolo, R. 2019, *ApJ*, 874, L21
- Ando, S., Cyburt, R. H., Hong, S. W., & Hyun, C. H. 2006, *Phys. Rev. C*, 74, 025809
- Angulo, C., Arnould, M., Rayet, M., et al. 1999, *Nuclear Physics A*, 656, 3
- Angulo, C., Casarejos, E., Couder, M., et al. 2005, *ApJ*, 630, L105
- Aver, E., Olive, K. A., & Skillman, E. D. 2015, *JCAP*, 7, 011
- Bania, T. M., Rood, R. T., & Balsaer, D. S. 2002, *Nature*, 415, 54
- Broggini, C., Canton, L., Fiorentini, G., & Villante, F. L. 2012, *JCAP*, 6, 030
- Brown, T. A. D., Bordeanu, C., Snover, K. A., et al. 2007, *Phys. Rev. C*, 76, 055801
- Caughlan, G. R., & Fowler, W. A. 1988, *Atomic Data and Nuclear Data Tables*, 40, 283
- Chakraborty, N., Fields, B. D., & Olive, K. A. 2011, *Phys. Rev.*, D83, 063006
- Charbonneau, P. 1995, *The Astrophysical Journal Supplement*, 101, 309
- Coc, A., & Davids, B. 2019, arXiv e-prints, arXiv:1912.03933

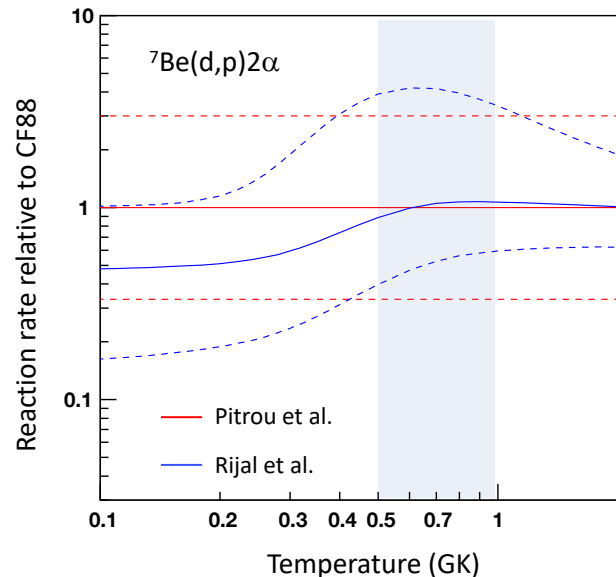


**Figure 10.** Rates of the  ${}^7\text{Be}(\text{d,p})2\alpha$  reaction normalized to the recommended rate (“CF88”) of [Caughlan & Fowler \(1988\)](#). Solid and dashed lines correspond to recommended rates and rate uncertainties, respectively. (Red) From [Pitrou et al. \(2018\)](#); since no uncertainty estimate was provided by [Caughlan & Fowler \(1988\)](#), a rate uncertainty factor of  $f.u. = 3$  was assumed. (Blue) From [Rijal et al. \(2019a\)](#). Notice that the results shown in red and blue are close to each other in the temperature range (shaded band) of primordial  ${}^7\text{Be}$  synthesis.

- Coc, A., Goriely, S., Xu, Y., Saimpert, M., & Vangioni, E. 2012, *ApJ*, 744, 158

- Coc, A., Petitjean, P., Uzan, J.-P., et al. 2015, *Physical Review D*, 92, 123526
- Coc, A., Uzan, J.-P., & Vangioni, E. 2014, *Journal of Cosmology and Astroparticle Physics*, 2014, 050
- Coc, A., Vangioni-Flam, E., Cassé, M., & Rabiet, M. 2002, *Phys. Rev.*, D65, 043510
- Coc, A., Vangioni-Flam, E., Descouvemont, P., Adahchour, A., & Angulo, C. 2004, *Astrophys. J.*, 600, 544
- Cooke, R. J., Pettini, M., & Steidel, C. C. 2018, *ApJ*, 855, 102
- Costantini, H., Bemmerer, D., Confortola, F., et al. 2008, *Nuclear Physics A*, 814, 144
- Cover, T. M., & Thomas, J. A. 2006, *Elements of Information Theory (Wiley Series in Telecommunications and Signal Processing)* (USA: Wiley-Interscience)
- Cuoco, A., Iocco, F., Mangano, G., et al. 2004, *Int. J. Mod. Phys.*, A19, 4431
- Cyburt, R. H., & Davids, B. 2008, *Phys. Rev.*, C78, 064614
- Cyburt, R. H., Fields, B. D., & Olive, K. A. 2003, *Physics Letters B*, 567, 227
- Cyburt, R. H., Fields, B. D., Olive, K. A., & Yeh, T.-H. 2016, *Rev. Mod. Phys.*, 88, 015004
- Davids, B. 2020, *Mem. Soc. Astron. Italiana*, 91, 20
- de Souza, R. S., Boston, S. R., Coc, A., & Iliadis, C. 2019a, *The Physical Review C*, 99, 014619
- de Souza, R. S., Iliadis, C., & Coc, A. 2019b, *The Astrophysical Journal*, 872, 75
- de Souza, R. S., Kiat, T. H., Coc, A., & Iliadis, C. 2020, *The Astrophysical Journal*, 894, 134
- Descouvemont, P., Adahchour, A., Angulo, C., Coc, A., & Vangioni-Flam, E. 2004, *Atomic Data and Nuclear Data Tables*, 88, 203
- di Leva, A., Gialanella, L., Kunz, R., et al. 2009, *Phys. Rev. Lett.*, 102, 232502
- Dubovichenko, S. B., Burkova, N. A., & Dzhazairov-Kakhramanov, A. 2018, *Indian Journal of Physics*, 1, copyright - Indian Journal of Physics is a copyright of Springer, (2018). All Rights Reserved; Last updated - 2018-09-18
- Dubovichenko, S. B., Burkova, N. A., & Dzhazairov-Kakhramanov, A. V. 2019, *Indian Journal of Physics*, 93, 279
- Dubovichenko, S. B., Burkova, N. A., & Dzhazairov-Kakhramanov, A. V., & Tkachenko, A. S. 2018, *Russian Physics Journal*, 60, 2077
- Ezhov, V. F., Andreev, A. Z., Ban, G., et al. 2018, *JETP Letters*, 107, 671
- Fields, B. D. 2011, *Annual Review of Nuclear and Particle Science*, 61, 47
- Fields, B. D., Olive, K. A., Yeh, T.-H., & Young, C. 2020, *Journal of Cosmology and Astroparticle Physics*, 2020, 010
- Fowler, W. A., Caughlan, G. R., & Zimmerman, B. A. 1967, *Annual Review of Astronomy and Astrophysics*, 5, 525
- Gai, M. 2019, arXiv e-prints, arXiv:1908.06451
- Gamow, G. 1948, *Nature*, 162, 680
- Gibson, S. E., & Charbonneau, P. 1998, *Journal of Geophysical Research*, 103, 14511
- Goldberg, D. E. 1989, *Genetic Algorithms in Search, Optimization and Machine Learning*, 1st edn. (USA: Addison-Wesley Longman Publishing Co., Inc.)
- Gómez Iñesta, A., Iliadis, C., & Coc, A. 2017, *ApJ*, 849, 134
- Holland, J. H. 1992, *Adaptation in Natural and Artificial Systems: An Introductory Analysis with Applications to Biology, Control and Artificial Intelligence* (Cambridge, MA, USA: MIT Press)
- Iliadis, C., Anderson, K. S., Coc, A., Timmes, F. X., & Starrfield, S. 2016, *ApJ*, 831, 107
- Iliadis, C., Longland, R., Coc, A., Timmes, F. X., & Champagne, A. E. 2015, *Journal of Physics G: Nuclear and Particle Physics*, 42, 034007
- Inoue, A., Tamii, A., Abe, K., et al. 2018, in *European Physical Journal Web of Conferences*, Vol. 184, European Physical Journal Web of Conferences, 02007
- Iocco, F., Mangano, G., Miele, G., Pisanti, O., & Serpico, P. D. 2009, *Phys. Rep.*, 472, 1
- Jurney, E. T., Bendt, P. J., & Browne, J. C. 1982, *Phys. Rev. C*, 25, 2810
- Kavanagh, R. W. 1960, *Nuclear Physics*, 18, 492
- Kirsebom, O. S., & Davids, B. 2011, *Phys. Rev.*, C84, 058801
- Korn, A. J., Grundahl, F., Richard, O., et al. 2006, *Nature*, 442, 657
- Kusakabe, M., Cheoun, M.-K., & Kim, K. S. 2014, *Phys. Rev. D*, 90, 045009
- Linfoot, E. H. 1957, *Information and Control*, 1, 85
- Longland, R. 2012, *Astronomy & Astrophysics*, 548, A30
- Mathews, G. J., Kusakabe, M., & Kajino, T. 2017, *International Journal of Modern Physics E*, 26, 1741001
- Michaud, G., Fontaine, G., & Beaudet, G. 1984, *ApJ*, 282, 206
- Moak, C. D. 1953, *The Physical Review*, 92, 383
- Mohr, P. J., Newell, D. B., & Taylor, B. N. 2016, *Rev. Mod. Phys.*, 88, 035009
- Nagai, Y., Kobayashi, T., Shima, T., et al. 2006, *Physical Review C*, 74, 025804
- Nara Singh, B. S., Hass, M., Nir-El, Y., & Haquin, G. 2004, *Phys. Rev. Lett.*, 93, 262503
- Neff, T. 2011, *Phys. Rev. Lett.*, 106, 042502

- Nollett, K. M., & Burles, S. 2000, *Phys. Rev. D*, 61, 123505
- Olive, K. A. 2010, ArXiv e-prints, arXiv:1005.3955
- Olive, K. A., Petitjean, P., Vangioni, E., & Silk, J. 2012, *MNRAS*, 426, 1427
- Olive, K. A., Steigman, G., & Walker, T. P. 2000, *Phys. Rep.*, 333, 389
- O'Malley, P. D., Bardayan, D. W., Adekola, A. S., et al. 2011, *Phys. Rev.*, C84, 042801
- Parker, P. D. 1972, *ApJ*, 175, 261
- Pattie, R. W., Callahan, N. B., Cude-Woods, C., et al. 2018, *Science*, 360, 627
- Peebles, P. J., & Ratra, B. 2003, *Reviews of Modern Physics*, 75, 559
- Pitrou, C., Coc, A., Uzan, J.-P., & Vangioni, E. 2018, *Physics Reports*, arXiv:1801.08023
- . 2019, arXiv e-prints, arXiv:1909.12046
- Planck Collaboration, Adam, R., Ade, P. A. R., et al. 2016, *A&A*, 594, A1
- Riess, A. G., Filippenko, A. V., Challis, P., et al. 1998, *AJ*, 116, 1009
- Rijal, N., Wiedenhöfer, I., Blackmon, J. C., et al. 2019a, *Physical Review Letters*, 122, 182701
- Rijal, N., Wiedenhöfer, I., Blackmon, J. C., et al. 2019b, *Phys. Rev. Lett.*, 123, 239902
- Sallaska, A. L., Iliadis, C., Champange, A. E., et al. 2013, *ApJS*, 207, 18
- Sbordone, L., Bonifacio, P., Caffau, E., et al. 2010, *A&A*, 522, A26
- Scholl, C., Fujita, Y., Adachi, T., et al. 2011, *Phys. Rev.*, C84, 014308
- Schramm, D. N., & Turner, M. S. 1998, *Reviews of Modern Physics*, 70, 303
- Serebrov, A. P., Kolomensky, E. A., Fomin, A. K., et al. 2018, *Phys. Rev. C*, 97, 055503
- Serpico, P. D., Esposito, S., Iocco, F., et al. 2004, *JCAP*, 2004, 010
- Singh, V., Lahiri, J., Bhowmick, D., & Basu, D. N. 2017, arXiv e-prints, arXiv:1708.05567
- Singh, V., Lahiri, J., Bhowmick, D., & Basu, D. N. 2019, *Journal of Experimental and Theoretical Physics*, 128, 707
- Smith, D. B., Jarmie, N., & Lockett, A. M. 1963, *The Physical Review*, 129, 785
- Spergel, D. N., Bean, R., Doré, O., et al. 2007, *ApJS*, 170, 377
- Spite, M., Spite, F., Caffau, E., & Bonifacio, P. 2015, *Astron. Astrophys.*, 582, A74
- Steigman, G. 2007, *Annual Review of Nuclear and Particle Science*, 57, 463
- Takács, M., Bemmerer, D., Junghans, A., & Zuber, K. 2018, *Nuclear Physics A*, 970, 78
- Tanabashi, M., Hagiwara, K., Hikasa, K., et al. 2018, *Phys. Rev. D*, 98, 030001
- Tišma, I., Lipoglavšek, M., Mihovilovič, M., et al. 2019, *The European Physical Journal A*, 55, 137
- Youn, L. G., Osetinskii, G. M., Sodnom, N., et al. 1961, *Soviet Physics JETP*, 12, 163